Topics in Catalysis Vol. 35, Nos. 3–4, July 2005 (© 2005)
DOI: 10.1007/s11244-005-3833-1

High activity TiO_2 photocatalysts prepared by a modified sol–gel method: characterization and their photocatalytic activity for the degradation of XRG and X-GL

Jiefang Zhu[a], Jinlong Zhang[a,*], Feng Chen[a] , Kiyoshi Iino[b] and Masakazu Anpo[b]

[a]*Lab for Advanced Materials and Institute of Fine Chemicals, East China University of Science and Technology, 130 Meilong Road, Shanghai 200237, P.R. China*

[b]*Department of Applied Chemistry, Graduate School of Engineering, Osaka Prefecture University, 1-1 Gakuen-cho, Sakai, Osaka 599-8531, Japan*

A simple method for preparing high photocatalytic activity TiO_2 has been developed by controlled the hydrolysis of titanium butoxide with water generated "i*n situ*" using an esterification reaction between the acetic acid and ethanol. The photocatalytic activity of the samples prepared was higher than that of the reference Degussa P25 TiO_2 for the liquid phase photocatatlytic degradation of active yellow XRG dye and cationic golden X-GL dye.

KEY WORDS: photocatalytic activity; esterification reaction; modified sol–gel method; TiO_2 (B).

1. Introduction

In recent years, titanium dioxide has been extensively used as an environmentally harmonious and clean photocatalyst due to its various merits, such as its optical and electronic properties, low cost, high photocatalytic activity, chemical stability and non-toxicity [1–5]. The photocatalytic activity of TiO_2 is dictated to a large extent by its crystal structure [6]. Generally, there are three crystalline phases for the TiO_2 photocatalyst: rutile, anatase and brookite. Rutile is a thermodynamically stable polymorph, but with low photocatalytic activity. Anatase, as one of the best kinetic products, has a higher photocatalytic activity than a rutile phase. Brookite is a naturally occurring phase and is relatively difficult to synthesize. In addition, it has been considered that a bicrystalline structure, containing anatase and rutile or anatase and brookite, has a higher photoactivity than either of the pure crystalline phases [7,8]. It is, therefore, scientifically and practically significant to explore new synthetic methods to prepare bicrystalline-phase or anatase TiO_2 in order to optimize the photocatalytic activity.

Among many preparation methods for TiO_2, the hydrolysis of titanium compounds such as titanium alkoxides and halides have been extensively employed. One of the difficulties in the hydrolysis of titanium compounds is the control of its rate. The traditional method of hydrolysis is based mainly on the physical introduction of water into the reaction system. Even when the solution of titanium compounds is stirred vigorously, the hydrolysis rate is so quick that large titania particles are precipitated once water is added. Recently, the hydrolysis method to prepare titania has been modified in some ways. When exposed to atmosphere, titanium alkoxides containing templates absorb moisture and subsequently hydrolyze to form porous titania materials [9,10]. Kominami *et al.* [11] have synthesized nanosized anatase TiO_2 by the hydrolysis of titanium (IV) alkoxide in toluene with water that was dissolved from the gas phase at high temperatures. These reactions took place at the interface between liquid and atmosphere, while the hydrolysis rates could be controlled by the atmospheric moisture or water vapor pressure. Esterification reactions have also been utilized to prepare TiO_2 by the hydrolysis of titanium alkoxides or halides since 1992 [12–16]. However, except Tseng *et al.* [16], no one has investigated the photocatalytic activity of titania prepared by this method. Furthermore, in this previous work, high temperature, high pressure and a long reaction time were required. These difficulties in the synthetic routes have been much improved and for the easy preparation of TiO_2 in our present studies.

In the present work, nanosized TiO_2 photocatalysts were prepared by controlling the hydrolysis of titanium butoxide through an esterification reaction between acetic acid and ethanol, as shown in equation (1). For a comparison of the photocatalytic activity, other esterifications between formic acid and propanol, isopropanol or n-butyl alcohol were also investigated. The photocatalytic activity of all the samples prepared was then investigated by the photocatalytic degradation of active yellow XRG dye and cationic golden X-GL dye.

$$\begin{gathered} CH_3CH_2OH + CH_3COOH \xrightarrow[55^{\circ}C]{H_2SO_4} H_2O + CH_3COOCH_2CH_3 \\ \downarrow \\ Ti(OBu)_4^+ H_2O \rightarrow Ti(OH)_4 + BuOH \end{gathered} \tag{1}$$

* To whom correspondence should be addressed.
E-mail: jlzhang@ecust.edu.cn

1022-5528/05/0700–0261/0

2. Experimental

2.1. Preparation of photocatalysts

For simplicity, four sets of codes are used to represent the four series of catalysts in this paper, as follows: A, B, C and D, as detailed below. Accordingly, the samples are denoted as A, B, C or D-*x*, where *x* indicates the calcination temperature of these samples.

A: Titanium *n*-butoxide (TNB, 98%) was hydrolyzed through the esterification reaction between acetic acid and ethanol. All the synthetic experiments were performed in a water bath at 55 °C. Twenty-five milliliter of TNB (0.0735 mol) was dissolved in 50 mL of anhydrous ethanol (0.858 mol) for 30 min, and then were mixed with 40 mL of acetic acid (0.699 mol) under mild stirring. When 4 mL of sulfuric acid (0.0724 mol) was added, the hydrolyzing water was homogeneously and equably released by the esterification of ethanol and acetic acid. After stirring the transparent mixture for 30 min, white titanium hydroxide precipitates were gradually produced. The resulting mixture was stirred for 2 h, aged for 2 h and filtrated. The filter residue was rinsed with ethanol and deionized distilled water repeatedly, dried at 80 °C for 6 h in order to remove most of ethanol and water, and then ground to fine powders in agate mortar to obtain dried gels. The dried gels were calcined in air for 6 h at 400, 450, 500, 550, 600, 650, 700, 750 and 800 °C, respectively, to obtain the nanosized TiO_2 photocatalysts of series A.

B: Titanium *tert*-isopropoxide (TTIP, Acros 98 + %) was hydrolyzed through an esterification reaction between formic acid and propanol. All the synthetic experiments were performed at room temperature. Ten milliliter of TTIP (0.0334 mol) was dissolved in 48 mL propanol (0.642 mol) for 30 min, and then mixed with 13 mL formic acid (0.535 mol) under mild stirring. After stirring the transparent mixture for 20 min, white titanium hydroxide precipitates were gradually produced. The resulting mixture was then stirred for 2 h, aged for 2 h and filtrated. The filter residue was rinsed with propanol and deionized distilled water repeatedly, dried at 80 °C, and then ground to fine powders in agate mortar to obtain dried gels. The dried gels were calcined in air for 6 h at 400, 450, 500, 550, 600 and 650 °C, respectively, to obtain the nanosized TiO_2 photocatalysts of series B.

C: TTIP was hydrolyzed through the esterification reaction between formic acid and isopropanol. All the synthetic experiments were performed at room temperature. Ten milliliter of TTIP (0.0334 mol) was dissolved in 50 mL of isopropanol (0.642 mol) for 30 min, and then mixed with 13 mL of formic acid (0.535 mol) under mild stirring. After stirring the transparent mixture for 30 min, white titanium hydroxide precipitates were gradually produced. The resulting mixture was stirred for 2 h, aged and filtrated. The filter residue was rinsed with isopropanol and deionized distilled water repeatedly, then dried, ground and calcined, as detailed in procedures for series B.

D: TNB was hydrolyzed through the esterification reaction between formic acid and *n*-butyl alcohol. All the synthetic experiments were performed at room temperature. Ten milliliter of TNB (0.0294 mol) was dissolved in 52 mL of n-butyl alcohol (0.546 mol) for 30 min, and then mixed with 11 mL of formic acid (0.470 mol) under mild stirring. After stirring the transparent mixture for 40 min, white titanium hydroxide precipitates gradually were produced. The resulting mixture was stirred for 4 h, aged and filtrated. The filter residue was rinsed with n-butyl alcohol and deionized distilled water repeatedly, then dried, ground and calcined, as detailed in series B.

2.2 Characterization of photocatalysts

XRD measurements were carried out with a Rigaku D/max 2550 VB/PC apparatus at room temperature using Cu K_α radiation and a graphite monochromator, operating at 40 kV and 100 mA. The crystallite sizes of the samples were determined using Cu $K_{\alpha 1}$ radiation (1.5406 Å) at 40 kV and 200 mA, and calculated from the half-height width of the different diffraction peaks of anatase and rutile using the Scherrer equation [17]. High-purity silicon powder (99.9999%) was used as an internal standard material to account for the instrumental line broadening effect during crystal size estimation. The UV–Vis diffuse reflectance spectra (DRS) were obtained for the dry-pressed disk samples using a Scan UV–Vis–NIR spectrophotometer (Varian Cary 500) equipped with an integrating sphere assembly, using $BaSO_4$ as the reference sample. The spectra were recorded at room temperature in air, in the wavelength range of 200 ~ 800 nm. The BET specific surface areas (S_{BET}) of the samples were determined through nitrogen adsorption at 77 K (Micromeritics ASAP 2010). All the samples were degassed at 473 K before measurement. The diffusion reflectance Fourier transform infrared (FT-IR) spectroscopy experiments were performed on a Nicolet Magna 550 spectrometer with a KBr beam splitter. The spectra were collected with a resolution of 4 cm^{-1} with 100 scans. The Raman spectra were obtained with a Raman spectrometer (Dilor, Super LabRam. II), using the excitation wavenumber at 785 nm with an output power of 3 mW. High-resolution transmission microscopy (HRTEM) (FEI, TECNAI 20 at 200 kV) was carried out to investigate the microstructure of A-450°C while the point to point resolution was 2 Å. For HRTEM observations, the sample powders were dispersed in ethanol by 10 min ultrasonic irradiation, and a drop of the suspension was placed onto a carbon-coated copper grid. The deposit was dried in air prior to observation. Energy-dispersive X-ray

spectroscopy (EDS) (EDAX, Falcon at 15 kV) was used to analyze the surface chemical composition of some of the samples in series A. Thermogravimetry (TG) and differential thermal analysis (DTA) (Mettler Toledo TGA/SDTA851[e]) were conducted at a rate of 10 °C min^{-1} from 20 °C to 1000 °C under air flow (60 ml min^{-1}).

2.3 Photocatalytic activity

The photocatalytic activity of each sample was measured in terms of the degradation of active yellow XRG dye and cationic golden X-GL dye (schemes 1 and 2). XRG and X-GL were selected because of their well-defined optical absorption characteristics and good resistance to light degradation. 0.06 g of each catalyst was suspended in 60 mL of standard XRG or X-GL aqueous solution (200 mg L^{-1} of XRG, 50 mg L^{-1} of X-GL) using a 70 mL-capacity quartz tube for each sample. The catalysts were agitated for 1 h in dye solution in the absence of light to attain the equilibrium adsorption on the catalyst surface. UV irradiation was carried out using a 300 W high-pressure Hg lamp, with the strongest emission at 365 nm. The distance between the light and the reaction tube was 20 cm. Samples of 3.5 mL were withdrawn every 30 min, and the catalysts were separated from the suspensions by filtration through 0.22 μm cellulose membranes. The quantitative determinations of the dyes were performed by measuring their absorption at 386 nm for XRG and 438 nm for X-GL, with a UV–Vis spectrophotometer (Varian Cary 100). The extent of the photodegradation of the dyes was calculated using a calibrated relationship between the measured absorbance and concentration. Each photodegradation was repeated three times, and the average was adopted. The margin for error in these determinations was found to be lower than 5%. XRG did not show photodegradation in the absence of a catalyst under the same irradiation conditions, while only 3% of X-GL (50 mg·L^{-1}) could be photodegraded directly after 2 h irradiation. Moreover, no further degradation of XRG and X-GL, except limited absorption on the surface of the samples, was observed in the dark.

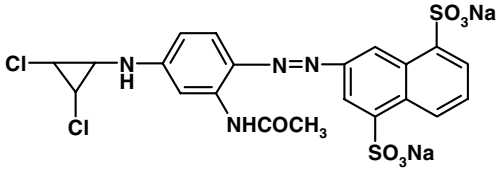

Scheme 1. Molecular structure of XRG

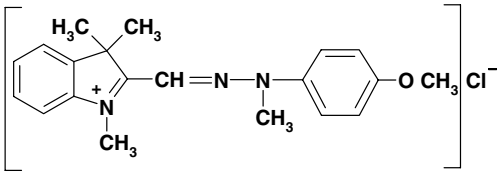

Scheme 2. Molecular structure of X-Gl.

3. Results and Discussion

3.1. XRD patterns

The XRD patterns for the catalysts of series A are shown in figures 1 and 2. The dried TiO_2 gel powders were amorphous, while the gels were crystallized to the anatase phase (JCPDS 21-1272) by calcinations, as depicted in figure 1. The crystallite size and crystallinity of anatase increased gradually with the calcination temperature, as shown in figure 1 and table 1. Interestingly, weak peaks for TiO_2 (B) (JCPDS 35-88), an uncommon crystal phase of TiO_2, were found in the samples calcined at 400, 450, 500 and 550 °C. Unfortunately, it is very difficult to obtain pure TiO_2 (B), since it is a very rare crystal phase of TiO_2. Hence, there has not been any empirical formula or standard curve to get the exact contents of anatase and TiO_2 (B). However, judging from the peak areas of the anatase and TiO_2 (B), the relative content of TiO_2 (B) attains a maximum at 450 °C calcination. The TiO_2 (B) was slowly transformed into anatase at higher temperatures, and disappeared completely at 600 °C, which is a little lower than the value in literature [18,19]. This may be ascribed to the fact that the heat produced by the combustion of residue bidentate acetates and sulfates, which cannot be removed completely at 400 °C, as shown in Table 1 and reported elsewhere [20–22], promote the transformation of TiO_2 (B). Steric effects induced from large stable acetates and sulfates support the formation of loose zigzag chains in octahedra coordination in the TiO_2 (B) [23] and anatase, as compared with linear chains of octahedra in rutile. The interstitial spaces between the octahedra in TiO_2 (B) and anatase are, therefore, larger,

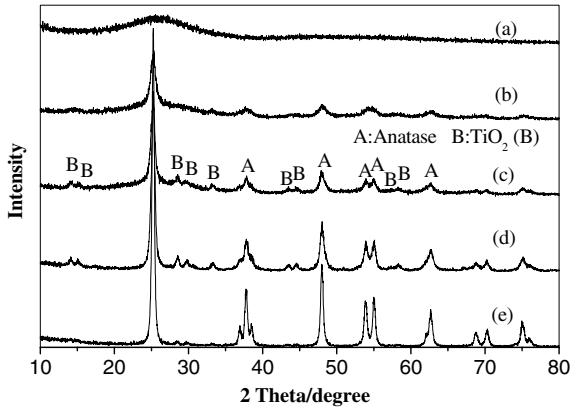

Figure 1. XRD patterns of (a) dried TiO_2 gel powders of Series A, (b) A-400 °C, (c) A-450 °C, (d) A-500 °C and (e) A-550 °C.

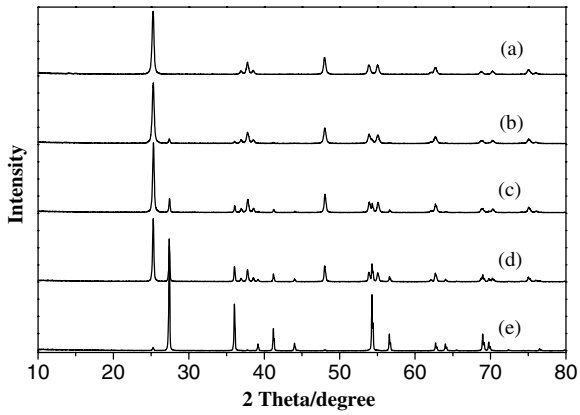

Figure 2. XRD patterns of (a) A-600 °C, (b) A-650 °C, (c) A-700 °C, (d) A-750 °C and (e) A-800 °C.

making them less compact than rutile and brookite (densities of TiO_2 (B) and anatase are 3.64 g cm^{-3} and 3.84 g cm^{-3} respectively, as compared with 4.26 g cm^{-3} for rutile and 4.17 g cm^{-3} for brookite).

A-600 °C was pure anatase, as shown in figure 2. When the samples were calcined at higher temperatures, transformation from anatase to rutile (JCPDS 21-1276) and an increase in the crystallite size occurred. At up to 800 °C, most of anatase disappeared. It is noteworthy that in the same sample, the crystallite size of rutile is always larger than that of anatase. Hence, it can be supposed that the phase transformation to rutile was initiated after the anatase grains had grown to a certain size. The critical nuclei size for rutile formation could be estimated at 50 nm from this study. Once the critical nuclei size had been attained from anatase grain growth during heat treatment, rapid rutile formation and grain growth were observed, so that the resulting rutile grains were larger than the coexisting anatase grains. In addition, XRD patterns indicated that the samples in series B, C and D were completely transformed into rutile at 600 °C or lower temperatures (not shown here). The residual and stable sulfates may be responsible for the relatively high thermal stability of anatase in series A [24–26]. The pH of the zero point of the charge (pH_{ZPC}) for the TiO_2 powders is generally in a range between 5.1 and 6.7. Below pH_{ZPC} in the preparation system of series A, the TiO_2 precipitate is of positive charge. Sulfates, which are of negative charge, can be strongly absorbed and bonded onto the surface of the TiO_2 precipitate. Thus, the electrostatic and steric repellence induced by small amounts of sulfates can keep TiO_2 particles from rapid growth and agglomeration, that is, before the thermal decomposition of sulfates, anatase grains can be of smaller size than the critical nuclei size for rutile formation.

3.2. UV–Vis diffuse reflectance spectra (UV–Vis DRS)

In figure 3, a steep decrease in the absorption at wavelengths longer than 380 nm can be assigned to the intrinsic bandgap absorption of pure anatase TiO_2. There are no distinct absorption edge shifts with the different calcination temperatures, indicating that these samples have similar crystallite sizes. Perhaps due to the low concentration of TiO_2 (B) in these samples or the same bandgap of TiO_2 (B) as anatase, the effect of TiO_2 (B) can not be found in the UV–Vis diffuse reflectance spectra. In addition, S-doped TiO_2 have been prepared recently [27,28]. The dopant was incorporated either as S^{2-} to take the place of oxygen in the lattice of TiO_2, or as S^{6+} to replace the titanium. In both cases, the absorption of visible light was obviously enhanced by

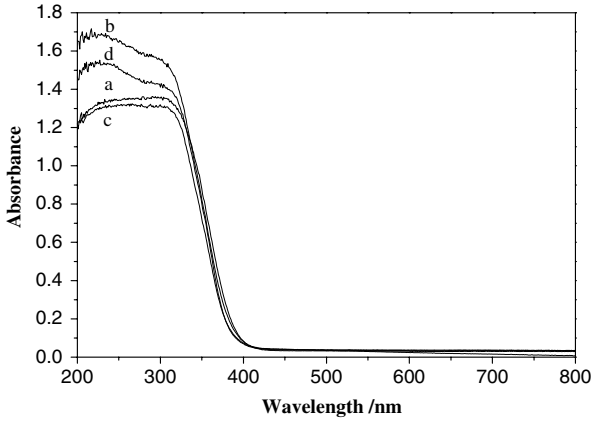

Figure 3. Diffuse reflectance spectra of (a) A-400 °C, (b) A-450 °C, (c) A-500 °C and (d) A-550 °C.

Table 1
Physicochemical properties and photocatalytic activities of some of the samples in series A

Sample	Anatase crystallite (Size /nm)[a]	S_{BET} /m^2 g^{-1}	C:O:S:Ti (At%)[b]	Degraded XRG (%)[c]	Degraded X-GL (%)[c]
A-400 °C	11.7	53.52	5.34:65.82:8.62:20.22	68.0	36.9
A-450 °C	13.9	51.81	1.40:63.20:1.80:33.60	97.6	69.9
A-500 °C	15.5	76.92	1.36:62.95:1.18:34.51	94.9	69.5
A-550 °C	22.7	47.67	1.11:61.95:0.44:36.50	90.6	82.5

[a]Determined by XRD using the Scherrer equation.
[b]Determined by EDS. The measured C content is a little higher than the actual value, due to the effect of the background of the carbon film.
[c]After photodegradation for 2 h, excluding the equilibrium adsorption. The value for P25 is 91.4%.

doping S, and then S-doped TiO_2 induced photocatalytic activity under visible light irradiation. However, the photocatalytic activity under UV light irradiation, as adopted in our present work, was not enhanced in those cases. Furthermore, no effect of residual S on the optical absorption was found, as shown in figure 3. The direct effect of the residual S on the photocatalytic activity may be negligible.

3.3. HRTEM images

HRTEM was used to investigate the exact microstructure of A-450 °C, as shown in figure 4. The sizes of the crystallites were 12 ~ 16 nm, corresponding closely to the sizes estimated by XRD analysis (table 1). The uniform crystallites with nearly spherical or globular morphology are a little aggregated, which decreases the S_{BET} of the samples (table 1). The slight aggregation may be partly promoted by the combustion of the residue acetates and sulfates during calcination. There is also a little amorphous phase in this sample. In figure 4(a), the lattice fringes of grain 1 have a spacing of 5.82 Å, very close to the lattice spacing of the (200) planes of TiO_2 (B), and accordingly, this grain can be identified as the TiO_2 (B) structure. The lattice fringes of the 2, 3 and 4 grains have a spacing of 3.54 Å, simultaneously close to those of the (101) planes of anatase and the (100) planes of TiO_2 (B). From the XRD patterns, it was found that anatase was the major phase. In figure 4(b) of the same specimen, the lattice fringes with a spacing of 5.82 Å in grain 1 corresponded to the (200) planes of TiO_2 (B), analogously a lattice spacing of 6.25 Å in grain 2 and 3.13 Å in grain 3 corresponded to the (001) and (002) planes of TiO_2 (B), respectively. These grains have the same phase as TiO_2 (B). The lattice spacing of 3.54 Å in the 4, 5 and 6 grains corresponded either to the (101) planes of anatase or to the (100) planes of TiO_2 (B). Figure 4 shows the coexistence of anatase and TiO_2 (B), in good agreement with the XRD investigations.

3.4. Raman spectra

The results of the laser Raman spectra are shown in figure 5. In figure 5, the peaks at around 139 cm^{-1} (e_g), 194 cm^{-1} (e_g), 393 cm^{-1} (b_{1g}), 513 cm^{-1} (b_{1g}) and 636 cm^{-1} (e_g) of A-600 °C can be assigned to anatase [29,30]. Only a weak peak at 140 cm^{-1} (e_g) can be observed clearly in A-400 °C, indicating its poor crystallinity. It was observed that most of the peaks of the Raman spectra shifted to red and become intense due to the increasing particle size and crystallinity with the higher calcination temperature. Peaks at around 120 cm^{-1}, 234 cm^{-1}, 251 cm^{-1} and 360 cm^{-1} can be observed from sample A-500 °C, while these peaks are not exhibited for A-600 °C and some of them emerge weakly with A-400 °C. As shown in table 1, there are little impurities in the samples calcined at temperatures higher than 450 °C, therefore, these peaks may be assigned to TiO_2 (B), coinciding with the results of the XRD patterns.

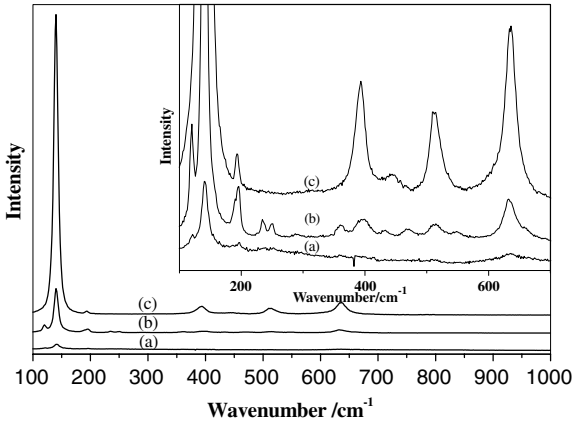

Figure 5. Raman spectra of (a) A-400 °C, (b) A-500 °C and (c) A-600 °C. The inset curves depict the magnified range from 100 to 700 nm.

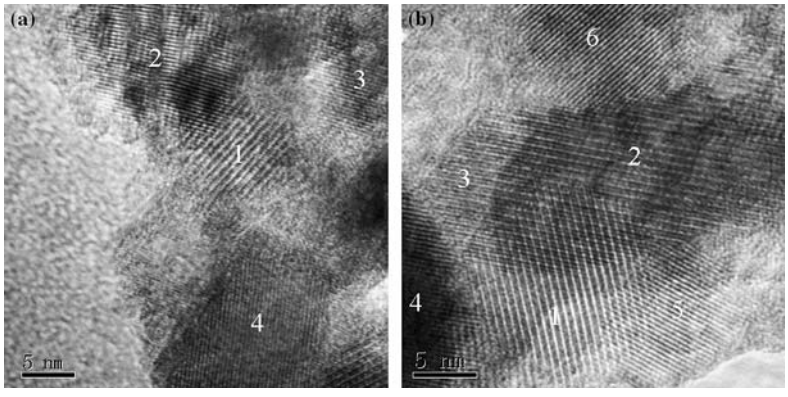

Figure 4. HRTEM images of A-450 °C.

3.5. EDS and S_{BET} determination

It can be seen from table 1 that a considerable amount of compounds containing S and C exist in A-400 °C. They can be removed gradually by calcination at high temperatures. A small amount of sulfates can inhibit TiO_2 particles from growth and agglomeration. Hence, after the sulfates are decomposed completely at 600 °C, anatase grains grow rapidly, leading to the formation of a rutile phase and a dramatic decrease in S_{BET}, as shown in table 2.

3.6. TG/DTA

The TG/DTA curves of the dried TiO_2 gel powers of series A are presented in figure 6. The observed weight loss can mainly be divided into three parts. The first is centered at 110 °C of about 14% and corresponds to the vaporization of the adsorbed water and ethanol, accompanied by an endothermic peak. The second is from 465 °C to 525 °C and can be assigned to the combination of chelating acetates [21,31] along with an exothermic peak. The last started at 540 °C and can be ascribed to the decomposition of sulfates [32] while being associated with a sharp endothermic peak. Due to the relatively rapid heating-up rate in TG/DTA, some of the above phenomena slightly lag behind those for EDS. Two exothermic peaks centered at 335 °C and 670 °C result from the transformation heats of an amorphous part to an anatase phase and anatase to rutile, respectively.

3.7. FT-IR analysis

The bands at 3425 and 1630 cm^{-1} correspond to the stretching and bending vibrations of –OH of the absorbed water molecular and hydroxyl groups linked to TiO_2, and which decreased rapidly upon calcination. The bands at 2343 cm^{-1} in A-400 °C and A-450 °C may be assigned to the stretching vibration of C≡C or C=C=C from the carbonization of the chelating acetates. When the calcination temperature was higher, the chelating acetates were completely combusted and the vibration bands vanished. The broad peak at 1250 ~ 1000 cm^{-1} can be ascribed to the superposition of the signals of SO_4^{2-} and Ti–O–C [25,31], which is

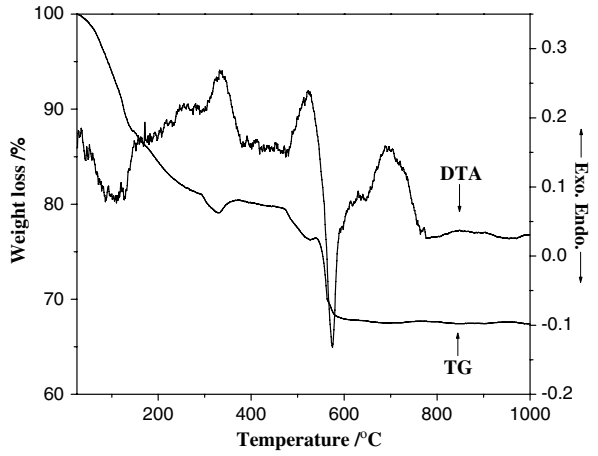

Figure 6. TG/DTA curves for the dried TiO_2 gel powders for series A.

obviously weaken by calcination at 500 °C. The band at 460 °cm^{-1} due to Ti–O vibration of TiO_2 becomes stronger with higher calcination temperature (figure 7).

3.8. Photocatalytic activity

The photocatalytic activity of the samples prepared and the reference P25 (Degussa) was determined by the

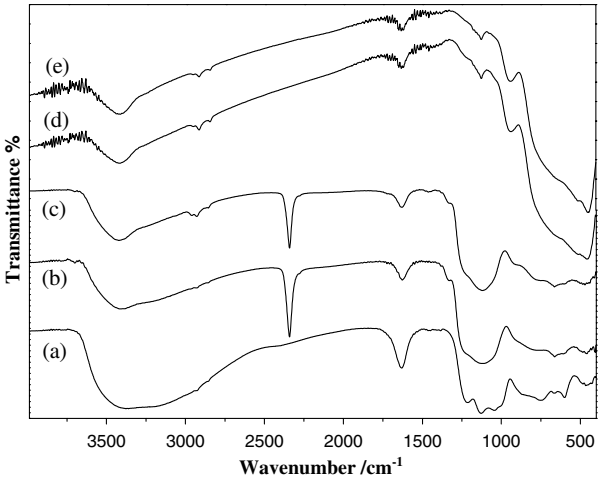

Figure 7. FT-IR spectra of (a) dried TiO_2 gel powders of series A, (b) A-400 °C, (c) A-450 °C, (d) A-500 °C and (e) A-550 °C.

Table 2
Physicochemical properties and photocatalytic activities of some of the samples in series A

Sample	Anatase crystallite (Size /nm)[a]	Rutile crystallite (Size /nm)[a]	Anatase content (%)[a]	S_{BET} (/m^2 g^{-1})	Degraded XRG (%)[b]	Degraded X-GL (%)[b]
A-600 °C	29.0	–	100	52.95	95.0	90.7
A-650 °C	27.7	50.4	94.30	38.50	95.7	92.7
A-700 °C	37.4	60.7	85.44	23.27	96.2	85.4
A-750 °C	45.5	64.3	64.23	13.32	96.8	77.1
A-800 °C	80.0	> 100	2.26	4.10	39.1	55.7

[a]Determined by XRD.
[b]After photodegradation for 2 h, excluding the equilibrium adsorption. The value for P25 is 91.5%.

photocatalytic degradation of XRG and X-GL, as shown in figures 8 and 9. This degradation of XRG and X-GL follows apparent 0~1 order kinetics, depending on the photocatalytic activity of a certain sample (not shown here). Highly efficient degradation, photocatalyzed by most of samples in series A, was observed pseudo first-order kinetics, while slower degradation, induced by the samples in series B, C and D, preferably followed pseudo zero-order kinetics, which may be dominated by electron–hole recombinations [33]. It can be seen from figures 8 and 9 that in a wide range of calcination temperatures, the samples in series A have a high photocatalytic activity with some and some more photoactive than P25, a well known photocatalyst of high photoactivity. In combination with the XRD patterns, it can be concluded that both a bicrystalline phase containing major anatase and minor TiO_2 (B) or rutile, and pure anatase TiO_2 favorably exhibit high photoactivity. The low photoactivity of A-400 °C is due to its relatively poor crystallinity and too many impurities, such as acetates and sulfates, while the poor photoactivity of A-800 °C can be ascribed to the high content of rutile. As for series B, C and D, due to the thermal instability of anatase, only when in a very narrow range of the calcination temperature, the samples show high crystallinity, purity, and anatase content simultaneously, which leads to relatively good photcatalytic activity in these series. Comparing figures 8 and 9, it was found that the relative photoactivity of some samples slightly differs with the photodegraded dye, even when the same series of photocatalysts are studied. These results may indicate that the optimal crystalline phase composition and surface structure of the photocatalysts partly depend on the kind of photocatalytic reaction.

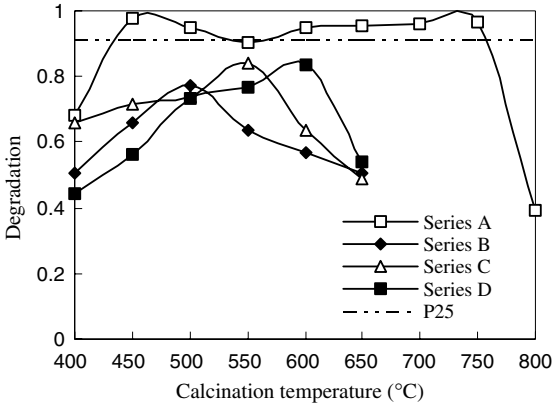

Figure 8. Photodegradation of XRG as a function of the calcination temperature. UV light irradiation time was 2 h.

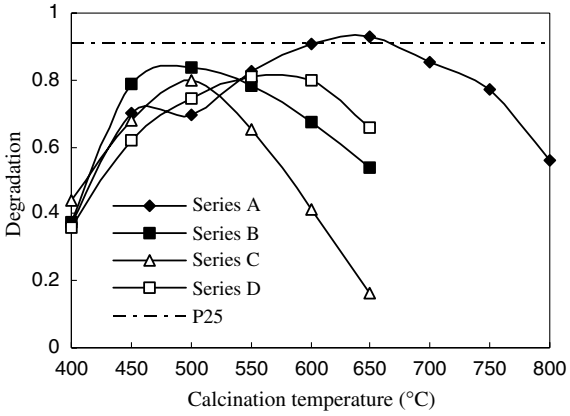

Figure 9. Photodegradation of X-GL as a function of the calcination temperature. UV light irradiation time was 2 h.

The high photocatalytic activity of the samples in series A may also be due to the sulfates and acetates used. On the one hand, a small amount of sulfate can stabilize the anatase phase and the S_{BET} against calcinations, that is, the transformation temperature from anatase to rutile shifted towards higher temperatures in series A. Consequently, the bicrystalline and pure anatase phase formed in a wide range of calcination temperatures contributed to high photoactivity. On the other hand, in the preparation system of series A, the acetate can act as a chelating ligand and modify the precursor TNB at the molecular level (scheme 3) [21], which contributes to the formation of monodisperse precipitates and uniform particles, even after calcination [34,35]. In addition, the chelating acetates are less easily hydrolyzed than the OBu groups, which increased the time of gelation and favored the polycondensation process [31], accordingly providing a superior condition for the nucleation and growth of the TiO_2 primary particles in solution. After hydrolysis, some actetates still remained in the dried TiO_2 gels. They could only be removed by calcination at a high temperature [21,31]. In addition, the time for precipitation in the preparation process of series D was longer than that for series A due to the slower esterification reaction between the formic acid and n-butyl alcohol, rather than a slower hydrolysis for TNB.

In figure 10, a set of photocatalytic degradation curves has been selected to illustrate the photocatalytic effect of the samples in series A. The peak at 468 nm decreases upon irradiation due to the destruction of the

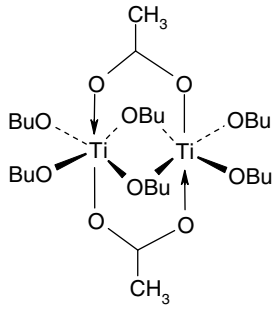

Scheme 3. Complex structure between CH_3COOH and $Ti(OBu)_4$.

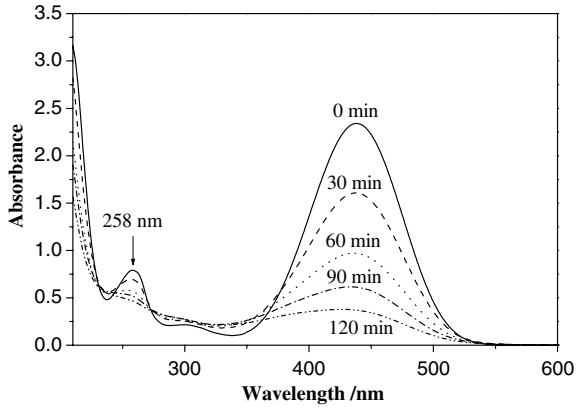

Figure 10. Absorbance of X-GL aqueous solution (50 mg L^{-1}) as a function of the irradiation time, using A-700 °C as the photocatalyst.

conjugated system in X-GL. The absorptions at around 258 and 210 nm, corresponding to the photostable aromatic derivates in X-GL, have also decreased obviously through photoctalytic degradation. This phenomenon may indicate that X-GL can be considerably mineralized by the samples in series A.

4. Conclusions

High photocatalytic activity TiO_2 were prepared by a modified sol–gel method in which the hydrolysis of the titanium butoxide was controlled through an esterification reaction between acetic acid and ethanol. An uncommon bicrystalline phase of anatase and TiO_2 (B) could be obtained by this method within a suitable temperature range of calcination. The modified homogeneous hydrolysis process may result in producing uniform crystallites and in enhancing the photocatalytic activity of the prepared TiO_2 powders. Furthermore, the acetates and sulfates in the preparation system were also found to be responsible for the high photocatalytic activity of the prepared samples. A small amount of residual sulfates worked to stabilize the anatase phase and the S_{BET} against calcinations, while acetate acted as a chelating ligand to modify the precursor TNB, resulting in a slow hydrolysis rate and the formation of uniform TiO_2 particles. The prepared photocatalysts could efficiently decompose the aromatic substrates of X-GL.

Acknowledgments

This work has been supported by the National Nature Science Foundation of China; Shanghai Nanotechnology Promotion Center and Commission of Education of Shanghai.

References

[1] M.A. Fox and M.T. Dulay, Chem. Rev. 93 (1995) 341.
[2] M.R. Hoffmann, S.T. Martin, W. Choi and D.W. Bahnemann, Chem. Rev. 95 (1995) 69.
[3] A.L. Linsebigler, G. Lu and J.T. Yates Jr., Chem. Rev. 95 (1995) 735.
[4] A. Fujishima, T.N. Rao and D.A. Truk, J. Photochem. Photobiol. C: Photochem. Rev. 1 (2000) 1.
[5] M. Anpo and M. Takeuchi, J. Catal. 216 (2003) 505.
[6] D.R. Park, J.L. Zhang, K. Ikeue, H. Yamashita and M. Anpo, J. Catal. 185 (1999) 114.
[7] R.I. Bickley, T. Gonzalez-Carreno, J.S. Lees, L. Palmisano and R.I.D. Tilley, J. Solid State Chem. 92 (1991) 178.
[8] J.C. Yu, J. Yu, W. Ho and L. Zhang, Chem. Comm. 19 (2001) 1942.
[9] S.-H. Feng, R.-R. Xu, C.G. Judith, J. Wijnhoven and W.L. Vos, Science 281 (1998) 802.
[10] A. Imhot and D.J. Pine, Adv Mater 11 (1999) 311.
[11] H. Kominami, S. Murakami, Y. Kera and B. Ohtani, Catal. Lett. 56 (1998) 125.
[12] A. Larbot, I. Laaziz, J. Marignan and J.F. Quinson, J. Non-Cryst. Solids 147&148 (1992) 157.
[13] M. Ivanda, S. Musiç, S. Popoviç and M. Gotiç, J. Mol. Struct. 480–481 (1999) 645.
[14] C. Wang, Z.-X. Deng and Y. Li, Inorg. Chem. 40 (2001) 5210.
[15] W. Liu, A.-P. Chen, J.-P. Lin, Z.-M. Dai, W. Qiu, W. Liu, M.-Q. Zhu and S. Usuda, Chem. Lett. 33 (2004) 390.
[16] I.H. Tseng, J.C.S. Wu and H.Y. Chou, J. Catal. 221 (2004) 432.
[17] B.D. Cullity, *Elements of X-Ray Diffraction* (Addison-Wesley, Reading, MA, 1978).
[18] R. Marchand, L. Brohan and M. Tournoux, Mat. Res. Bull. 15 (1980) 1129.
[19] M. Tournoux, R. Marchand and L. Brohan, Prog. Solid State Chem. 17 (1986) 33.
[20] S. Doeuff, M. Henry, C. Sanchez and J. Livage, J. Non-Cryst. Solids 89 (1987) 206.
[21] S. Takenaka, R. Takahashi, S. Sato and T. Sodesawa, J. Sol–Gel Sci. Tech. 19 (2000) 711.
[22] S. Yamazaki, N. Fujinaga and K. Araki, Appl. Catal. A: Gen. 210 (2001) 97.
[23] Y. Bando, M. Watanabe and Y. Sekikawa, Acta. Cryst. B35 (1979) 1541.
[24] G. Colón, M.C. Hidalgo and J.A. Navío, Appl. Catal. B: Environ. 45 (2003) 39.
[25] S.K. Samantaray, P. Mohapatra and K. Parida, J. Mol. Catal. A: Chem. 198 (2003) 277.
[26] R. Gómez, T. López, E. Ortiz-Islas, J. Navarrete, E. Sánchez, F. Tzompanztzi and X. Bokhimi, J. Mol. Catal. A: Chem. 193 (2003) 217.
[27] T. Umebayashi, T. Yamaki, S. Tanaka and K. Asai, Chem. Lett. 32 (2003) 330.
[28] T. Ohno, T. Mitsui and M. Matsumura, Chem. Lett. 32 (2003) 364.
[29] J. Zhang, T. Ayusawa, M. Minagawa, K. Kinugawa, H. Yamashita, M. Matsuoka and M. Anpo, J. Catal. 198 (2001) 1.
[30] Y. Iida, M. Furukawa, T. Aoki and T. Sakai, Appl. Spectrosc. 52 (1998) 673.
[31] S. Doeuff, M. Henry, C. Sanchez and J. Livage, J. Non-Cryst. Solids 89 (1987) 206.
[32] G. Colón, M.C. Hidalgo and J.A. Navío, Appl. Catal. B: Environ. 45 (2003) 39.
[33] A.-W. Xu, Y. Gao and H.-Q. Liu, J. Catal. 207 (2002) 151.
[34] P. Gherardi and E. Matijevic, J. Colloid Interf. Sci. 109 (1986) 57.
[35] E. Matijevic, Ann. Rev. Mater. Sci. 15 (1985) 483.